is determined by the spanwise lift distribution, and the lift during pitch-up will be greater than that during pitch-down at a given angle of attack. The circulation curve for $0.5C$ illuminates this trend; the circulation during pitch-up is greater than that during pitch-down at a given angle of attack. However, the curve for $1.5C$ is contrary to this. This discrepancy can be explained if we take into account the fact that the velocity signal sensed at $1.5C$ reflects the data originated at an earlier phase angle of the wing oscillation. The true phase angles (hence, the true angles of attack) for the data for 0.5 and $1.5C$ are different from each other. For an adequate comparison we therefore need to take into account the phase lag of the present measurement. To compensate for the phase lag, we assumed that the convection velocity was approximately equal to the mean axial velocity in the tip vortex region at $0.5C$. We fitted the mean axial velocity data averaged over the vortex core region at several angles of attack into two straight lines, one for pitch-up and the other for pitch-down. The convection velocity at an angle of attack of interest was then obtained from these straight lines.

The phase lag compensated plot of the data is given in Fig. 4b. Obviously, at a given angle of attack the circulation during pitch-up is greater than that during pitch-down as expected. Figure 4b also points out that the rates of increase or decrease of the vortex strength per unit angle of attack are about the same for both pitch-up and pitch-down. This signifies that the rate of increase of the vortex strength per unit angle of attack remains the same even when the mean flow is massively separated. The value of circulation for $\alpha = 7$ deg during pitch-up from the phase lag compensated curve (Fig. 4b) is read to be about 0.23, which is in close agreement with the value of 0.28 (at $1.5C$) for $\alpha = 7$ deg of the stationary wing test.[12] Takahashi and McAlister[15] investigated the tip vortex in the near field of a stationary wing at $R_N = 1.02 \times 10^6$. The normalized circulation at large radius in their work was 0.33 at $\alpha = 11$ deg and $X/C = 1.6$. The value from the phase lag compensated curve (Fig. 4b) is about 0.37. This, in a way, ascertains that the flow during pitch-up is similar to that of the stationary wing in the present range of experiment. The circulation at various angles of attack for $X/C = 0.5$ and that for $X/C = 1.5$ are seen to be a little different from each other. However, these two can be said to be about the same if we take the measurement uncertainty into consideration. The uncertainties of circulation for $\alpha = 15$ deg during pitch-up were about ± 11.8, $\pm 9.5\%$ at 0.5 and $1.5C$, respectively.

Conclusion

Phase-averaged mean axial and tangential velocity profiles in the near field of the trailing vortex behind an oscillating wing were presented. These velocity profiles clearly demonstrated hysteretic behavior of the wake. The flow during the pitch-down motion was more disturbed and irregular so that it was more diffusive. The size of the vortex core was larger, and the peak tangential velocity and the axial velocity deficit were smaller during pitch-down than during pitch-up. The axial velocity within the vortex region was found to suffer from velocity deficit for both pitch-up and pitch-down cases. The hysteretic behavior of the wake was best illustrated in the plot showing the variation of the circulation over one cycle of oscillation. To adequately describe the change of circulation during a cycle of oscillation, the phase lag of the measurement signal was taken into account. The phase lag compensated variation of the vortex strength over one cycle of oscillation showed that the circulation at a given angle of attack was greater during pitch-up than during pitch-down. The rates of increase or decrease of the vortex strength per unit angle of attack, however, were found to be about the same for both pitch-up and pitch-down motion.

References

[1]Ramaprian, B. R., and Zheng, Y., "Measurements in Rollup Region of the Tip Vortex from a Rectangular Wing," *AIAA Journal*, Vol. 35, No. 12, 1997, pp. 1837–1843.

[2]Shekarriz, A., Fu, T. C., Katz, J., and Huang, T. T., "Near-Field Behavior of a Tip Vortex," *AIAA Journal*, Vol. 31, No. 1, 1993, pp. 112–118.

[3]Higuchi, H., Quadrelli, J. C., and Farell, C., "Vortex Roll-up from an Elliptic Wing at Moderately Low Reynolds Numbers," *AIAA Journal*, Vol. 25, No. 12, 1987, pp. 1537–1542.

[4]Bandyopadhyay, P. R., Stead, D. J., and Ash, R. L., "Organized Nature of a Turbulent Trailing Vortex," *AIAA Journal*, Vol. 29, No. 10, 1991, pp. 1627–1633.

[5]Green, S. I., and Acosta, A. J., "Unsteady Flow in Trailing Vortices," *Journal of Fluid Mechanics*, Vol. 227, 1991, pp. 107–134.

[6]Devenport, W. J., Rife, M. C., Liapis, S. J., and Follin G. J., "The Structure and Development of a Wing-Tip Vortex," *Journal of Fluid Mechanics*, Vol. 312, 1996, pp. 67–106.

[7]Dacles-Mariani, J., Zilliac, G. G., Chow, J., and Bradshaw, P., "Numerical/Experimental Study of a Wing-Tip Vortex in the Near Field," *AIAA Journal*, Vol. 33, No. 9, 1995, pp. 1561–1568.

[8]Chow, J. S., Zilliac, G. G., and Bradshaw, P., "Mean and Turbulence Measurements in the Near Field of a Wing Tip Vortex," *AIAA Journal*, Vol. 35, No. 10, 1997, pp.1561–1567.

[9]Ramaprian, B. R., and Zheng Y., "Near Field of the Tip Vortex Behind an Oscillating Rectangular Wing," *AIAA Journal*, Vol. 36, No. 7, 1998, pp. 1263–1269.

[10]Triantafyllou, M. S., Triantafyllou, G. S., and Gopalkrishnan, R. J., "Wake Mechanics for Thrust Generation in Oscillating Foils," *Physics of Fluids A*, Vol. 3, No. 12, 1991, pp. 2835–2837.

[11]Bandyopadhyay, P. R., and Donnelly, M. J., "The Swimming Hydrodynamics of a Pair of Flapping Foils Attached to a Rigid Body," *High Speed Body Motion in Water*, R-827, AGARD, 1998.

[12]Chang, J. W., and Park, S. O., "An Experimental Study of Tip Vortex Roll-Up of an Oscillating Wing," AIAA Paper 99-0142, Jan. 1999.

[13]Chang, J. W., and Park, S. O., "A Visualization Study of Tip Vortex Roll-up of an Oscillating Wing," *Journal of Flow Visualization and Image Processing*, Vol. 6, 1999, pp. 79–87.

[14]Thompson, D. H., "Experimental Study of Axial Flow in Wing Tip Vortices," *Journal of Aircraft*, Vol. 12, No. 11, 1975, pp. 910, 911.

[15]Takahashi, R. K., and McAlister, K. W., "Preliminary Study of a Wing-Tip Vortex Using Laser Velocimetry," NASA TM 88343, 1987.

P. R. Bandyopadhyay
Associate Editor

Application of Acoustic Analogy to Automotive Engine-Cooling Fan Noise Prediction

Jeonghan Lee,* Kyungseok Cho,* and Soogab Lee†
Seoul National University,
Seoul 151-742, Republic of Korea

Nomenclature

c_0	= speed of sound
h	= blade surface equation $h = 0$, where $h > 0$ outside the blade
l_i	= force per unit area exerted on the fluid by the solid surface (in x_i direction)
l_r	= $l_i \hat{r}_i$, force per unit area exerted on the fluid in the radiation direction
M	= local Mach number
M_i	= local Mach number in x_i direction
M_r	= $M_i \hat{r}_i$, local Mach number in the radiation direction
N_{blade}	= number of blades
N_p	= number of singularity panels in potential flow solver
N_t	= number of time steps in potential flow solver
p'	= acoustic pressure
R	= fan radius
R_w	= wake radius
r	= $\lvert \boldsymbol{x} - \boldsymbol{y} \rvert$, where $\boldsymbol{y}$ is the source position
$\hat{r}_i$	= unit radiation vector, $(\boldsymbol{x} - \boldsymbol{y})/r$
S	= surface area of the actual body $h = 0$
t	= observer time

Received 10 September 1998; revision received 15 October 1999; accepted for publication 14 February 2000.

*Graduate Student, School of Mechanical and Aerospace Engineering.

†Professor, School of Mechanical and Aerospace Engineering. Member AIAA.

$\boldsymbol{x}$ = observer position
$\Gamma_{\max}$ = maximum circulation
ρ_0 = ambient density of air
Φ = velocity potential
ϕ = angle between the tip vortex and the plane of blade rotation

Subscripts

i, j = 1, 2, or 3
L = dipole, loading component
r = radiation direction
ret = evaluation at retarded time
T = monopole, thickness component

Introduction

ACOUSTIC consideration of axial fans has become imperative because of regulations and the ubiquitous call for environment-friendly products. Although the dominant source of noise for most axial fans is known to be dipole (because of surface pressure fluctuations) in nature, the formidability of flowfield calculations have kept many attempts of analysis to only those of empirical formulations. The rapid advances in computer technology have, however, motivated the development of a noncompact fan noise analysis tool with the flowfield data from the accompanying flow analyzer. The main challenge in this venture lies in bridging the gap between the two different timescales involved in solving for the flowfield and the acoustic field. The tool couples time-domain acoustic analogy with flowfield analysis via the free-wake panel method. The time-domain acoustic prediction uses one of the most rigorous formulations and is implemented for use in predicting aerodynamic noise of the most complex geometry often found in axial fan blades. A time-stepping, free-wake potential solver is tested for flowfield calculation of an automotive cooling fan.

Although free-wake panel methods usually yield relatively accurate results when predicting the flowfield around axial fans, its use in aerodynamic noise prediction has been limited by two shortcomings. The time resolution of flow analysis is usually of an order larger than that required for noise predictions. The free-wake panel method also suffers from wake instabilities in the absence of freestream as in static fan operations. Because the two problems are not irrelevant, a solution is sought that will resolve the two problems at once. The prediction method is applied to an axial fan operating with shroud, and the resulting noise predictions show a favorable agreement with the measured data.

Numerical Formulations

Farassat and Succi[1] have formulated the following equation, which is very convenient in embodying the time-domain analysis of the Ffowcs Williams–Hawkings equation into a computer code. The formulation does not lose the generality of being able to handle blades of arbitrary shape and motion while enhancing the accuracy of the code by eliminating numerical time differentiation. The field pressure is given by

$$p'(\boldsymbol{x}, t) = p'_T(\boldsymbol{x}, t) + p'_L(\boldsymbol{x}, t) \tag{1}$$

where $p'_T(\boldsymbol{x}, t)$ and $p'_L(\boldsymbol{x}, t)$ represent thickness and loading terms, respectively, and correspond to the monopole and dipole terms in the theory of acoustic analogy. The quadrupole source from Lighthill stress tensor T_{ij} is neglected in this study because only low-speed rotating blades are considered. The monopole term is also neglected because the airfoil is thin and because the tip speed is not high enough to cause any significant noise through volume displacement of fluid. The loading term is given by

$$4\pi p'_L(\boldsymbol{x}, t) = \frac{1}{c_0}\int_{h=0}\left(\frac{\dot{l}_i \hat{r}_i}{r(1-M_r)^2}\right)_{\text{ret}} \mathrm{d}s + \int_{h=0}\left(\frac{l_r - l_i M_i}{r^2(1-M_r)^2}\right)_{\text{ret}} \mathrm{d}s + \frac{1}{c_0}\int_{h=0}\left(\frac{l_r\left(r\dot{M}_i\hat{r}_i + c_0 M_r - c_0 M^2\right)}{r^2(1-M_r)^3}\right)_{\text{ret}} \mathrm{d}s \tag{2}$$

where the dots on $\dot{M}_i$ and $\dot{l}_i$ represent the rate of change with respect to source time.

A computer program has been developed taking full advantage of the formulation. The calculations are performed on the surface of the blade, which is divided into a number of panels used for integration. The primary convenience of the formulation lies in the fact that other than the retarded time calculation, which in the subsonic case is simple with Newton iteration, the coding is straightforward with all of the terms in the integrand calculated in the blade fixed frame.

The flow solver is a classic potential flow solver, using singularity panels on the body surfaces and the wakes trailing from the bodies. If the flow is assumed inviscid, incompressible, and irrotational, the velocity potential of the flow must satisfy Laplace's equation $\nabla^2\Phi = 0$. The establishment of algebraic equations is well documented in various literatures[2] and will not be iterated here. The free-wake panel method derives its name from the principle in which the wake panels are free to evolve in shape according to the velocities dictated by the solution. The free wake is time stepped, with a new row of panels shed into the flow with each time step. Increase in temporal resolution of the flow solution is thus equivalent to additional computation of velocities at the new panel points with the number of calculations proportional to $N_p^2 N_t$. Therefore, the CPU time scales approximately with the cube of the number of time steps. For the flow data to be used as input for acoustic calculation, pressure data per less than 10 deg are required, whereas for flow-only calculations pressure data per over 10 deg usually suffice. The time-resolution refinement then places a heavy burden on the computer capacity, requiring a way to use fewer wake panels to simulate the wake field. The problem of wake instability commonly observed in rotating blades must also be addressed. The instability of the wake is mainly caused by numerical errors and partially reflects the physics that flowfield of axial fans are indeed turbulent. The instability can be inhibited by introducing numerical damping, which in this case is attained by increasing the core value of the wake. Using smaller time steps, however, one is able to use smaller core values leading to more realistic wake geometry. But even with the smallest time steps, correct wake geometry cannot be obtained if the far wake is not modeled correctly.

An ultimate wake sink disk is introduced to overcome these problems. Helical vortex lines representing rolled-up vortices can be replaced by a sink disk on the cap of a circular cylinder with ring vortices.[3] The strength of the sink disk is given by $N_{\text{blade}}\Gamma_{\max}/2\pi R_w \tan\phi$. Replacing the infinite extent of tip vortices with a sink disk reduces the calculation load drastically while providing the effect of far wake components. To prevent the number of wake panels from increasing indefinitely, the wake relaxation (discarding one panel while adding one on the other side) option is added to simulate the refined flowfield with as small a number of wake panels as possible.

Results and Discussion

The automotive cooling fan used for result validation is shown in Fig. 1. Ten divisions in the radial direction were used, whereas 20 divisions were used to wrap around the airfoil. The shroud is also modeled with 80 divisions around the circumference to simulate as closely as possible the actual flowfield of the fan. The initial

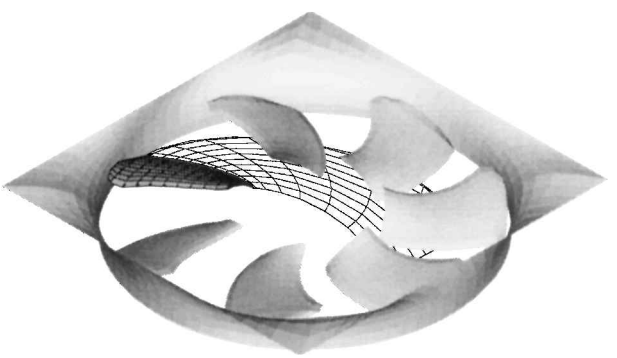

Fig. 1 Fan geometry with initial wake panels (only the inner surface of shroud shown).

wake geometry is also shown. The wake sink disk, not shown, is placed $1.5R$ away from the plane of blade revolution. The location was chosen from observing a tentative low-resolution calculation, which indicated piling up of wake panels in the vicinity. The radius of the sink disk is $0.8R$, considering the contraction of the wake. With the wake disk accounting for the far wake effect, a flowfield calculation of high temporal resolution is carried out with an interval of 3 deg (120 calculations per revolution). The core value used in this calculation is 5% of the fan radius. The resulting wake geometry is shown in Fig. 2 via the boundaries of singularity panels representing vorticity. Only the inner and tip boundaries of the wake sheet are shown for clarity.

Figure 3 shows the predicted and measured acoustic spectra at a number of locations. The actual sound-pressure-level (SPL) values are not specified, but each division represents a difference of 3.0 dB. The four graphs are plotted with respect to the same scale so that the directivity of the noise propagation can be estimated. The frequency data are A-weighted. The noise is measured in an anechoic chamber measuring $5 \times 5 \times 3.8$ m, with a cutoff frequency of 80 Hz and a background noise level of less than 20 dB(A). The spectrum is obtained through B&K 4550 spectrum analyzer. The points of observation are varied keeping a constant distance of 1 m from the fan center. The increase in the overall noise level as the observer nears the axis of rotation is typical of the unsteady loading noise. Comparison of the results shows good agreement with the experimental data, especially for the first few harmonics of blade passing frequency. Of the discrete peaks in experimental data, the fourth harmonic shows a distinguished value, which is a result of modal interference of the seven-bladed fan and the four-cornered shroud. The overpredictions in the higher frequency range are the result of an insufficient number of panels used for shroud modeling, a further increase of which imposes a heavy burden on the computation time. The current version of the prediction code does not take into account the effects of diffraction and interference with the shroud of the fan, consideration of which could generate some complex phenomena.

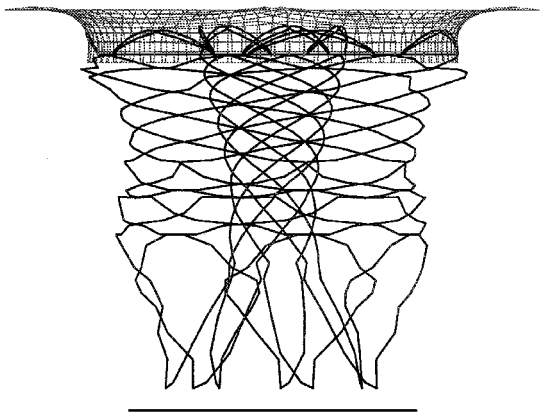

Fig. 2 Wake geometry showing the tip and the inboard boundaries of the vortex sheet.

Conclusion

Aerodynamic noise from an automotive cooling fan has been predicted using acoustic analogy in conjunction with the free-wake panel method. The timescale gap between the two methods has been bridged successfully. The prediction results agree well with the measured noise spectra, especially toward the axis of rotation where the unsteady dipole noise radiation is greatest. Further refinement of the prediction method is currently being sought through addition of structures such as hub and support struts that are present in a real situation.

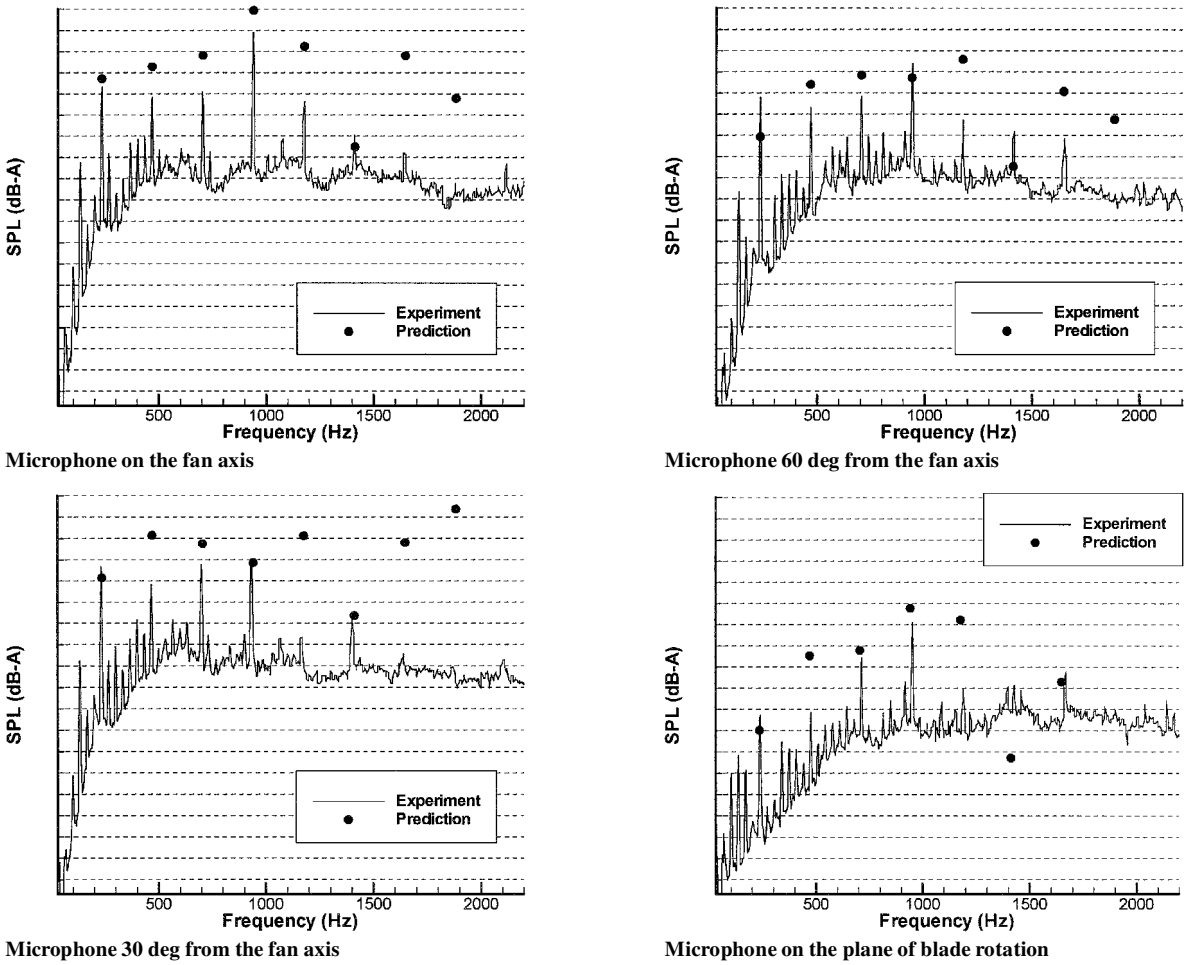

Microphone on the fan axis | **Microphone 60 deg from the fan axis**

Microphone 30 deg from the fan axis | **Microphone on the plane of blade rotation**

Fig. 3 Comparison of measured and predicted noise spectra, 1 m away from the hub center. (Each division in the SPL axis represents 3 dB, and all graphs are of equal range.)

References

[1]Farassat, F., and Succi, G. P., "The Prediction of Helicopter Rotor Discrete Frequency Noise," *Vertica*, Vol. 7, No. 4, 1983, pp. 309–320.

[2]Katz, J., and Plotkin, A., *Low-Speed Aerodynamics*, McGraw–Hill, New York, 1991, pp. 237–263.

[3]Lee, J., "A Potential Based Panel Method for the Analysis of Marine Propellers in Steady Flow," Ph.D. Dissertation, Dept. of Ocean Engineering, Massachusetts Inst. of Technology, Cambridge, MA, July 1987.

P. J. Morris
Associate Editor

Navier–Stokes Prediction of Internal Flows with a Three-Equation Turbulence Model

S. Duranti* and F. Pittaluga†
University of Genoa, 16145 Genoa, Italy

Nomenclature

G	= compressible shear-layer growth rate g normalized by its incompressible counterpart g_i ($G = g/g_i$; $g = \mathrm{d}\delta_\omega/\mathrm{d}x$)
K	= turbulent kinetic energy
K_ρ	= density variance ($K_\rho = \langle\rho'^2\rangle$)
M_C	= convective Mach number in a two-stream mixing layer ($M_C = \lvert U_1 - U_2\rvert/(a_1 + a_2)$, a being the sound speed)
U^*	= normalized X-component mean velocity [$U^* = (U - U_2)/(U_1 - U_2)$]; U_1 and U_2 are U in either stream of a two-stream mixing layer
$-\langle u'v'\rangle$	= Reynolds stress (ensemble mean)
V	= Y-component mean velocity
Y_2^*	= nondimensional y coordinate $\{Y_2^* = [(y - y_0)/\delta_\omega]\}$
δ_ω	= vorticity thickness $\{\delta_\omega = (U_1 - U_2)/[\partial U/\partial y]_{\mathrm{MAX}}\}$
ε	= dissipation rate
ρ'	= density fluctuation

Introduction

THE strategy most usually adopted for improving the numerical prediction of turbulent flows within the frame of classical K–ε, or similar, models is that of better calibrating these latter, or simply their coefficients, by pursuing interpretation of, or seeking accordance to, flow features such as velocity profiles, turbulence levels, dissipation rates, etc., with reference to specific flow situations. At difference with the preceding, the modelization effort here pursued numerically has been that of reinterpreting the classical two-equation turbulence model with the aim of capturing, at a fundamental level, the effects of the turbulence scales interaction: basically, this implies finding a proper analytical means suitable to represent the most relevant statistical quantities of the fluctuating field. In incompressible turbulence this strategy has already allowed both to improve the eddy viscosity formulation by taking care of the anisotropy of the turbulence field and to capture the higher-order effects in the shear-stress behavior.[1–3] In more general terms, it is here believed that the implications of the preceding perspective are very much promising and, at the same time, usually overlooked by the turbulence modelers, inducing the result that otherwise sophisticated schemes, such as the full Reynolds-stress models, turn out intrinsically weakened if this kind of statistical information is lacking. Such a point appears even more important when the turbulent flowfield is compressible or subject to thermally induced density variations.[4,5]

Navier–Stokes Solver with the Three-Equation Turbulence Model

To the said end, the approach adopted is the so-called TSDIA[1,4] method (two-scale direct-interaction approximation), extended with the latest compressible-turbulence developments [Markovianized two-scale method (MTS[5])]. Scale-expansion equations are written and solved directly in terms of fluctuations, and all of the involved correlations appear ready to be evaluated. Several correlations show up and require modelization, both in the governing Navier–Stokes equations and in the compressible-turbulence model: this latter turns out made up by a transport equation for each one of the three main turbulence quantities K, ε, K_ρ, namely the turbulent kinetic energy, the dissipation rate, and the density variance.[4–6]

From a numerical point of view, the preceding three-equation turbulence model has been implemented into a new version of NAST,[6,7] a three-dimensional time-dependent Navier–Stokes structured solver belonging, at large, to the Arbitrary Lagrangian–Eulerian codes' family, of which the series of Kiva[8] codes are the main representatives. To implement correctly the turbulence model has required conversion of the Favre averages previously adopted in NAST into ensemble-mean expressions: it is exactly this procedure that allows us to explicitly arrive at the fluctuating-field correlations to be modeled via the TSDIA/MTS methodologies, yielding a second-order representation of the Reynolds stresses.[4–6] In the last version of NAST, the governing equations are discretized explicitly for the diffusive and the convective terms, while an implicit Poisson-like pressure equation is obtained and solved via multigrid technique.[6]

Results and Discussion

A few comparisons are now presented between the (ensemble-mean) predictions of the NAST code and two turbulent test cases, one (numerical, direct numerical simulation) referred to as an isothermal, low-Mach-number, backward-step flow situation[8] and the other (experimental) to a compressible variable-property free-shear flow regime.[9] The complete results have recently been presented in all details.[6]

With reference to the first test case, the Reynolds number based on freestream velocity and height of the step is 5.1×10^3, whereas the Reynolds number based on momentum thickness is 6.67×10^2. The calculations were performed on a 161×71 rectangular mesh, with some grid coarsening for Y/H higher than 3.

Figures 1 and 2 show, respectively, the horizontal velocity component and the Reynolds shear stress. The picture turns out everywhere good and in many instances excellent. The normal Reynolds-stress

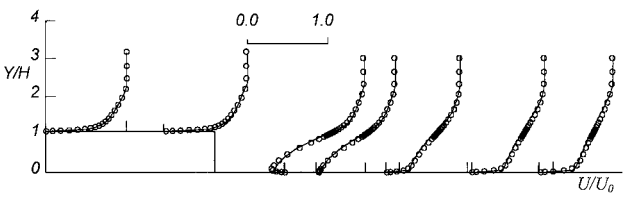

Fig. 1 Horizontal velocity (——, NAST; ∘, Le and Moin[9]).

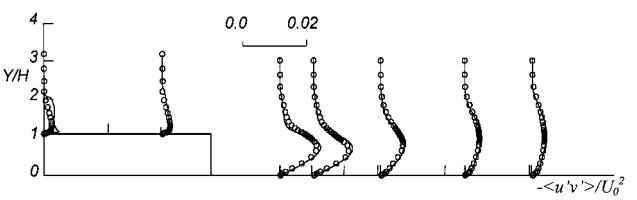

Fig. 2 Reynolds shear stress (——, NAST; ∘, Le and Moin[9]).

Received 22 June 1999; presented as Paper 99-3372 at the AIAA 14th Computational Fluid Dynamic Conference, Norfolk, VA, 28 June–1 July 1999; revision received 8 November 1999; accepted for publication 19 November 1999.

*Ph.D. Student, Department of Thermal Machines, Energy Systems, and Transportation.

†Professor, Department of Thermal Machines, Energy Systems, and Transportation. Associate Fellow AIAA.